Computationally Probing the Performance of Hybrid, Heterogeneous and Homogeneous Ir-based Catalysts for Water Oxidation

Max García-Melchor*[a], Laia Vilella[b], Núria López[c], Aleksandra Vojvodic*[d]

Abstract: An attractive strategy to improve the performance of water oxidation catalysts would be to anchor a homogeneous molecular catalyst on a heterogeneous solid surface to create a hybrid catalyst. The idea of this combined system is to take advantage of the individual properties of each of the two catalyst components. We use Density Functional Theory to determine the stability and activity of a model hybrid water oxidation catalyst consisting of a dimeric Ir complex attached on the IrO_2(110) surface through two oxygen atoms. We find that homogeneous catalysts can be bound to its matrix oxide without losing significant activity. Hence, designing hybrid systems that benefit from both the high tunability of activity of homogeneous catalysts and the stability of heterogeneous systems seems feasible.

Introduction

With the depleting nature of fossil fuels and the environmental concerns over their use, there exists an increasing necessity in replacing these energy sources by more sustainable and renewable ones.[1,2] One promising solution would be to use electrical energy from a renewable source, *e.g.* sunlight, and store it in the form of chemical bonds such as H_2 and O_2 through artificial photosynthesis.[3,4] The bottleneck of this process is the oxidation of water to molecular oxygen, also known as oxygen evolution reaction (OER).[5] This reaction is particularly energy demanding due to the mechanistic requirements in removing four electrons and protons from two water molecules with the concomitant formation of an O−O bond.[6,7] Hence, finding active OER catalysts that provide high current densities and further operate for substantial periods of time without degradation has been a quest for decades. To date, the best homogeneous and heterogeneous OER catalysts are based on iridium and ruthenium metals,[8–11] but the scarcity and high cost of these elements limit the ability of energy conversion technologies to be scaled up.[12] In addition, even the most active Ir- and Ru-based catalysts reported in the literature either require a high overpotential or are not stable enough for their industrial implementation. To overcome these issues, several approaches have been undertaken such as the synthesis of nature-inspired[13–15] and non-precious metal-based catalysts,[16–19] the addition of dopants[20–23] or promoters,[22,24,25] or the creation of confined reaction environments.[26,27]

Another appealing strategy, although very far from being fully exploited yet, consists in anchoring active homogeneous OER catalysts on a solid support (either active or inactive), thus creating a *hybrid-type* of catalyst.[28–31] The fundamental idea behind these integrated systems is that they might benefit from the individual properties of their homogeneous and heterogeneous constituents, as the limitations of ones are usually the main advantages of the others.[32] Homogeneous catalysts typically exhibit a high tunability of activity, but they lack the stability and good electron transport often found in heterogeneous catalyst systems. Besides the coexistence of these benefits, a synergistic effect arising from a combination of the two catalytic systems might also emerge. To date, a few successful examples of this strategy have been demonstrated including the very recent experimental studies on water oxidation using an Ir-based HEDTA catalyst supported on TiO_2,[33] and a dimeric Ir complex anchored on tin-doped indium oxide nanoparticles.[34] However, the interplay between the anchored molecular catalyst and the support remains still unknown.

Herein, we present the first Density Functional Theory (DFT) study on the OER performance (stability and activity) of a hybrid model Ir-based catalyst (Figure 1a) and compare it to its corresponding homogeneous and heterogeneous constituents (Figure 1b-c).

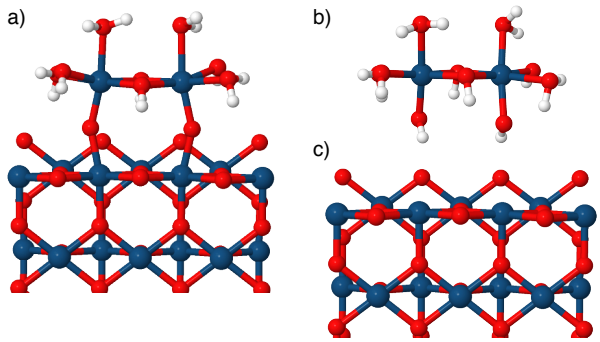

[a] M. García-Melchor*
Department of Chemical Engineering
SUNCAT Center for Interface Science and Catalysis
Stanford University, Stanford, CA 94305, USA.
maxg@slac.stanford.edu
[b] L. Vilella
Departament de Química
Universitat Autònoma de Barcelona
Cerdanyola del Vallès, E-08193 Barcelona, Spain.
[c] N. López
Institute of Chemical Research of Catalonia (ICIQ), Barcelona
Institute of Science and Technology (BIST)
Av. Països Catalans, 16, E-43007 Tarragona, Spain.
[d] A. Vojvodic*
SUNCAT Center for Interface Science and Catalysis, SLAC National Accelerator Laboratory
Menlo Park, CA 94025, USA.
alevoj@stanford.edu

Supporting information for this article is given via a link at the end of the document.

Figure 1. Side-view of the atomic structure for the investigated (a) hybrid, (b) homogeneous, and (c) heterogeneous Ir-based catalysts. Color code: Ir (dark blue), O (red), and H (white). This color code applies to all subsequent figures.

Our calculations show that the homogeneous catalyst binds strongly to the support surface and performs water oxidation without losing significant activity. We also identify the active site motifs and reaction pathways for each catalytic system, and based on that, propose that tuning the chemical properties of the surface can be used as a complementary approach to the metal ligand exchange to alter OER performance. These results may pave the way in the design of more efficient and robust water oxidation catalysts.

Computational Details

The stability and OER activity of the considered Ir-based catalysts have been investigated by means of DFT calculations in conjunction with the computational standard hydrogen electrode (SHE) model.[35] All the calculations have been performed using the Perdew-Burke-Ernzenhof[36] (PBE) exchange correlation functional as implemented in the VASP code, version 5.3.2.[37,38] Unless otherwise indicated, the core electrons of the Ir, O, and H atoms have been replaced by projector-augmented wave (PAW) pseudopotentials,[39] whereas their valence electrons have been expanded in plane waves with a kinetic energy cutoff of 450 eV.

The lattice parameters for the bulk rutile IrO_2 structure have been optimized using a higher cutoff energy of 600 eV and a 9×9×13 Monkhorst Pack (MP) k-point grid. The obtained lattice parameters are $a_{calc} = b_{calc} = 4.543$ Å and $c_{calc} = 3.187$ Å, which are in very good agreement with previous theoretical findings[40,41] and experimental values ($a_{exp} = b_{exp} = 4.505$ Å and $c_{exp} = 3.159$ Å).[42] To model the heterogeneous IrO_2 catalyst surface, we use a 2x1 supercell consisting of a slab of nine atomic layers of the most stable (110) facet[43] separated by at least 13 Å of vacuum. Geometry optimizations for this system have been carried out using a 5×5×1 MP k-point mesh and allowing the adsorbed species (O*, HOO*, OO*, H_2O* and HO*, where the asterisk corresponds to an active site on the oxide) and the five top-most atomic layers to relax, while keeping the rest of the atoms fixed at their bulk positions.

When it comes to the homogeneous catalyst, we simulate the dimeric complex $[Ir_2(H_2O)_4(OH)_4(\mu\text{-}OH)_2]$ using a cell of 18x15x15 Å in size and sampling the Brillouin zone at the Γ−point. This charge-neutral compound avoids the complexity of dealing with charged species in periodic calculations. To model the hybrid catalyst, we have anchored this dimeric Ir complex on top of the IrO_2(110) surface with a 6x2 periodicity through two oxygen atoms to the *cus* sites of the surface. Due to the considerable size of the combined system, calculations for this catalyst have been performed at the Γ−point. The energy convergence with respect to the k-point sampling has been examined for selected adsorbed species using a denser 2x3x1 k-point mesh, obtaining energy differences within 0.02 eV (Table S1). Geometry optimizations for the hybrid catalyst have been performed relaxing the OER intermediates, the atoms in the attached dimer, and the three top-most surface layers.

For the three model Ir catalysts, total energies have been converged to values smaller than 10^{-5} eV in the self-consistent field and geometries relaxed until the energy threshold of 10^{-4} eV has been fulfilled. The nature of all stationary points has been confirmed by calculating the vibrational frequencies of the adsorbed species and metal atoms directly coordinated to them. Contributions to the Gibbs energies for the adsorbates have been calculated at T = 300 K and p = 1 atm, except for water, for which the equilibrium vapor pressure at that temperature (p = 0.035 atm) has been used (see Supporting Information for details). The Gibbs energy for the water oxidation reaction has been fixed to the experimentally known value of 4.92 eV, in order to avoid introducing the DFT error in the energetics related to molecular oxygen.[35,44,45] Spin-polarized calculations have been carried out when needed, relaxing the total magnetic moment during the self-consistent cycles.
For the location of transition states, we have employed the climbing image nudged elastic band (CI-NEB) method using at least five images along the reaction coordinate.[46] The nature of these stationary points was assessed by performing numerical frequency analysis to confirm the existence of only one imaginary vibrational mode.

Results and Discussion

In this work, we investigate the viability of a hybrid water oxidation catalyst and the role of the surface in this type of system by anchoring the iridium complex $[Ir_2(H_2O)_4(OH)_4(\mu\text{-}OH)_2]$ on the IrO_2(110) surface through two oxygen atoms as linkers (Figure 1). We choose this dimeric Ir complex as homogeneous catalyst (Ir-hom) because it resembles the molecular species suggested to be involved in the formation of the purple-blue solution that catalyzes water oxidation.[47,48] Moreover, such a dimeric complex allows for comparison of the two main OER mechanisms proposed in the literature, namely the water nucleophilic attack (WNA) and the interaction between two M−O units (I2M).[11,49,50] On the other hand, as heterogeneous catalyst we select IrO_2 (Ir-het) because it is one of the most active pure single transition metal oxides reported to date,[9,51] and it has also been computationally studied in detail.[52–54]

We would like to note that the hybrid catalyst considered in this work (Ir-hyb) is intended to serve as a model to probe the feasibility and mechanistics of this type of systems, and should not be considered as a potential high-performance OER catalyst. With this aim, we first examine the stability of Ir-hyb by calculating the adsorption energy of the dimeric Ir complex to the IrO_2(110) surface as follows:

$$\Delta E_{ads} = E_{H2} + E_{Ir\text{-}hyb} - E_{Ir\text{-}hom} - E_{Ir\text{-}het} \qquad \text{(Eq. 1)}$$

where E_{H2}, $E_{Ir\text{-}hyb}$, $E_{Ir\text{-}hom}$, and $E_{Ir\text{-}het}$ are the potential energies for molecular hydrogen, and the Ir-hyb, Ir-hom and Ir-het systems, respectively. Importantly, the obtained adsorption energy from Eq. 1 is exothermic by 2.19 eV, indicating that indeed the dimeric Ir complex is strongly attached to the $IrO_2(110)$ surface through the two oxygen linkers. Interesting, the optimized Ir−Ir bond distance in the attached Ir dimer almost matches that distance of the $IrO_2(110)$ surface (3.207 versus 3.190 Å). Hence, this particular hybrid catalyst containing only aqua and hydroxo ligands might be conceived as a defect on the surface, or an extension of the $IrO_2(110)$ surface and, which would explain the strong interaction between its homogeneous and heterogeneous constituents predicted by calculations, or even possibly a crude model for amorphous IrO_x. Further insight into this interaction can be gained by evaluating the electronic charge density difference between the molecular and the surface fragments of the Ir-hyb catalyst (Figure S1). In fact, this analysis reveals that both Ir atoms from the adsorbed complex and the surface provide electron density to the O-linkers, thus making these bonds rather strong.

We also examine the stability of Ir-hyb by calculating the energy required to detach the dimeric Ir complex from the surface upon attack of two solvent water molecules, ΔE_{des}, according to the following equation:

$$\Delta E_{des} = E_{Ir\text{-}het+2OH} + E_{Ir\text{-}hom} - 2{*}E_{H2O} - E_{Ir\text{-}hyb} \qquad \text{(Eq. 2)}$$

where E_{H2O} and $E_{Ir\text{-}het+2OH}$ are the energies for a water gas molecule and the $IrO_2(110)$ surface with two OH groups adsorbed at *cus* positions, respectively. In this case, we find that the deactivation route in Eq. 2 is a highly endothermic process (1.54 eV), which reinforces the stability of the Ir-hyb system.

Before evaluating the OER activity for Ir-hyb and its individual constituents, it is necessary to determine the resting state of the catalyst under relevant reaction conditions. To this end, for each catalytic system we examined a number of potential species that might exist in aqueous solution. More specifically, for the Ir-het catalyst we have considered up to 19 different H, O, and OH surface coverages (Figure S2), and calculated their relative Gibbs energies as a function of *pH* and applied voltage (*U*), *i.e.* constructed a surface Pourbaix diagram. According to the Pourbaix representation (Figure 2a), the resting state for Ir-het under typical OER conditions corresponds to a surface with all Ir-*cus* sites completely covered by O atoms, in agreement with previous theoretical findings.[27,52]

Unlike the heterogeneous system, assessing the resting state for Ir-hom is significantly more complicated given the vast number of possible protonation states of this complex. However, a thorough analysis of the resting state for this system is still a necessity. Here, we tackle this issue by first exploring several consecutive dehydrogenations of Ir-hom at the thermodynamic potential of 1.23 V and *pH* = 0 (Figure S3). Under these conditions, calculations indicate that aqua ligands are preferentially dehydrogenated until a fully hydroxylated dimeric Ir(V) species is obtained (Figure S4). From this complex, we have further examined all possible isomers with different hydrogen content and formal Ir oxidation states up to +7 (Figure S5). It is worth mentioning that the existence of IrO_4 and $[IrO_4]^+$ species with oxidation states of +8 and +9 have been reported,[55,56] although they have been only characterized in rare-gas matrices. Therefore, we are only taking into account Ir species with oxidation states up to +7. The Pourbaix diagram constructed considering all the above dimeric Ir complexes (Figure 2b) shows that Ir-hom under OER overpotentials has a total of 6H atoms and corresponds to a symmetric Ir(VII)/Ir(VII) dimer with only hydroxo- and oxo-ligands in the equatorial and axial planes, respectively.

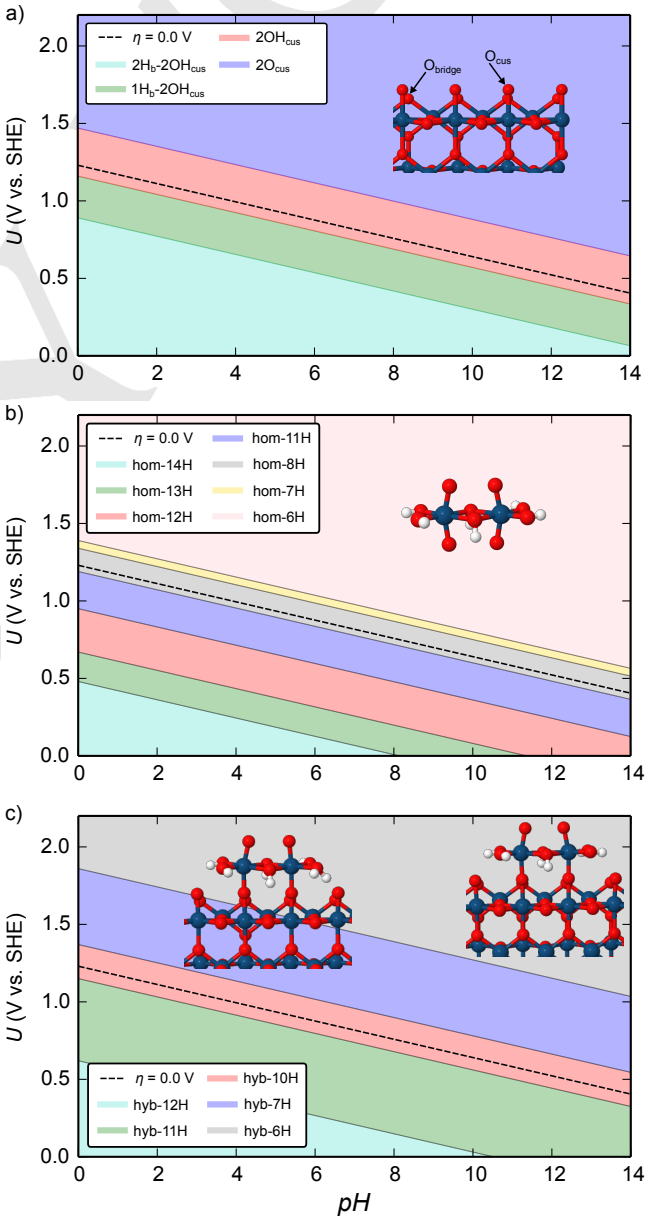

Figure 2. Calculated Pourbaix diagrams for the model (a) Ir-het, (b) Ir-hom, and (c) Ir-hyb catalysts. Insets of the most relevant structures are shown. The

coverages for the Ir-het system are labeled as mH_b-nOH_{cus}-kO_{cus}, where mH_b is the number of H atoms at the O_{bridge} positions, and mOH_{cus} and kO_{cus} are the number of OH and O groups in cus positions. Structures for the Ir-hom and Ir-hyb systems are named as nH, where n is the total number of H atoms contained in each system.

Due to the considerable size of the Ir-hyb catalyst, and the large number of possible protonation states of the adsorbed dimeric Ir complex, for this system we assume the same surface coverage as obtained for Ir-het (Figure 2a); that is, a surface with the *cus* sites fully covered by O atoms. As far as the resting state for the anchored Ir dimer is concerned, we have considered the same consecutive dehydrogenations as investigated for Ir-hom (Figure S3). Based on all these structures and several further oxidized species with formal Ir oxidation states up to +6, (Figure S6), we have constructed the Pourbaix diagram shown in Figure 2c. We find that there are two Ir-hyb species that might exist at relevant OER potentials (insets Figure 2c). The first one, stable at lower overpotentials, contains 7H atoms and corresponds to an Ir species with the equatorial plane fully hydroxylated except for one position that has an aqua ligand. The second one (denoted hyb-6H) is stable at slightly higher overpotentials and is analogous to the resting state found for Ir-hom. Interestingly, the potentials required to reach the same Ir oxidation states in Ir-hyb are significantly higher than the ones needed for Ir-hom, suggesting that Ir atoms of the Ir-hyb are less prone to be oxidized. We also find that, in contrast to the Ir-hom catalyst, the aqua ligands in the equatorial positions of Ir-hyb are more difficult to dehydrogenate due to the formation of H-bonds between these ligands and the O_{cus} surface atoms.

We next evaluate the OER activity for the Ir-het, Ir-hom and Ir-hyb catalysts based on the resting states derived from the Pourbaix diagrams (Figure 2). In order to compare the activity for these three catalytic systems, for each of them we have determined the potential-limiting step, defined as the onset potential at which all the OER steps become thermodynamically downhill. The difference between the limiting and the standard water oxidation potentials is the theoretical overpotential, η:[44,52,35]

$$\eta = \max(\Delta G_i/e) - 1.23\ V \qquad \text{(Eq. 3)}$$

For rutile oxides, water oxidation in acidic medium has been proposed to occur through a WNA mechanism[52,57,58] consisting of the following four electrochemical steps (WNA-1, Figure 3a):

(1) $H_2O\ (l) + O^* \rightarrow HOO^* + e^- + H^+$
(2) $HOO^* \rightarrow O_2\ (g) + * + e^- + H^+$
(3) $* + H_2O\ (l) \rightarrow HO^* + e^- + H^+$
(4) $HO^* \rightarrow O^* + e^- + H^+$

However, one variant of this mechanism would be to replace (2) and (3) by the following alternative steps that do not entail unsaturated octahedral Ir atoms at the surface (WNA-2, Figure 3a):

(2') $HOO^* \rightarrow OO^* + e^- + H^+$
(3') $OO^* + H_2O\ (l) \rightarrow O_2\ (g) + HO^* + e^- + H^+$

In this case, a proton-coupled-electron transfer (PCET) reaction from the HOO* intermediate yields a molecularly adsorbed OO* species that subsequently evolves to molecular oxygen and a HO* group generated via a second PCET. According to our calculations, the thermodynamically most energy demanding step in the WNA-1 mechanism corresponds to O_2 desorption, whereas in the WNA-2 it is the generation of the HOO* species (step 1), which involves the formation of the O−O bond. These reaction steps result in overpotentials of 0.61 and 0.40 V for the conventional WNA-1 and alternative WNA-2 mechanisms, respectively (Figure 3a). Thus, this alternative pathway is more favorable by 0.21 V, and therefore, we will consider this mechanism to compare the OER performance of Ir-het with the other mod-el catalysts. Moreover, the calculated overpotential of 0.40 V via the WNA-2 mechanism is in agreement with the

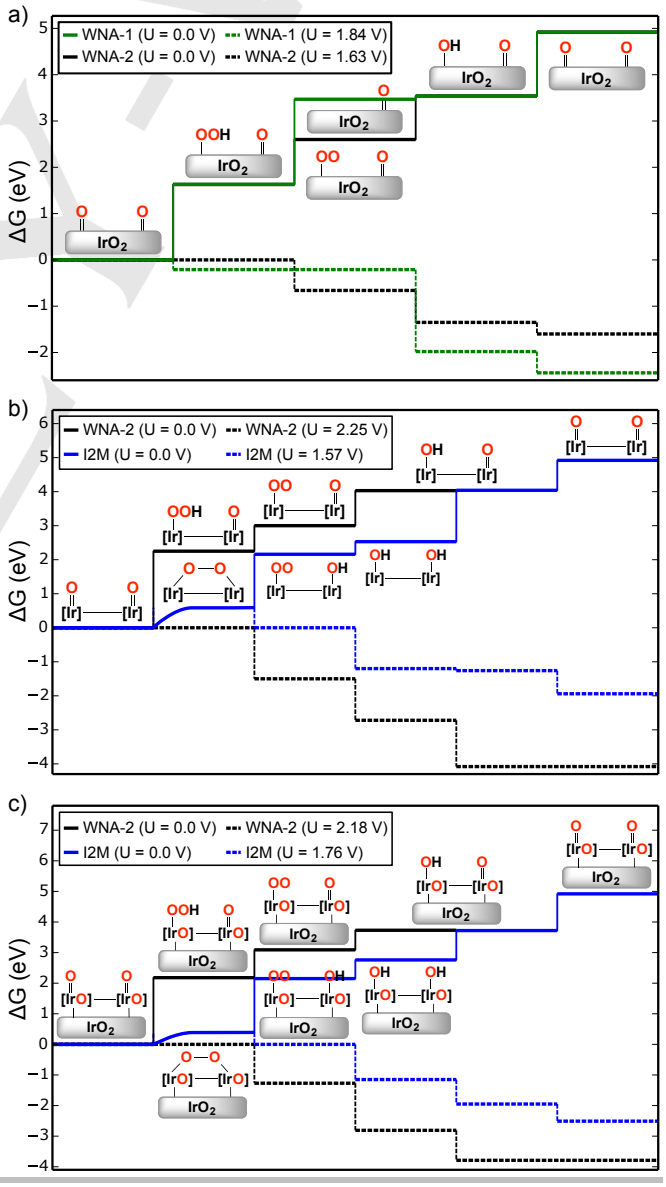

reported experimental value of 0.36 V at a current density of 10 mA/cm^2.[9]

Figure 3. Gibbs energy diagrams for the OER activity of the (a) Ir-het, (b) Ir-hom, and (c) Ir-hyb (with 6H atoms) catalysts via the conventional and alternative WNA (green and black lines, respectively) and I2M (blue lines) mechanisms.

For homogeneous water oxidation catalysts, both WNA and I2M reaction mechanisms have been shown to operate depending on the nature of the catalyst.[50] Thus, for Ir-hom we have explored these two mechanisms, as well as several variants of them (Figure S7). In the case of the WNA mechanism, we find that the lowest energy pathway is the same as for Ir-het (WNA-2, Figure 3a), with the O* → HOO* transition being the potential-limiting step (Figure 3b). Nevertheless, the calculated theoretical overpotential for Ir-hom is significantly higher, *i.e.* 1.02 V, as compared to Ir-het.

On the other hand, the lowest energy path obtained for the I2M mechanism consists of the next steps:

(1) O* + O* → *OO*
(2) *OO* + H_2O (l) → OO* + HO* + e^- + H^+
(3) OO* + HO* + H_2O (l) → 2HO* + O_2 (g) + e^- + H^+
(4) 2HO* → HO* + O* + e^- + H^+
(5) HO* → O* + e^- + H^+

This mechanism starts with the coupling between two iridium bis-oxo moieties leading to a μ-1,2-peroxo intermediate (Figure 3b). From this species, the cleavage of one Ir−O bond is promoted by the nucleophilic attack of a water molecule resulting in the formation of a superoxide and an OH group generated via PCET. This superoxide species subsequently evolves to molecular oxygen with the coordination of a second water molecule, which gives rise to an OH group through a second PCET. Finally, the starting bis-oxo species is regenerated after two consecutive PCET reactions, thus completing the catalytic cycle.

The potential at which all the electrochemical steps in the I2M mechanism become downhill in energy is 1.57 V (Figure 3b). However, a calculation of the transition state for the I2M mechanism reveals an activation barrier of 0.76 eV. To be noted is that this step is purely chemical, and thus it is not affected by the applied bias. The surmountable barrier together with the fact that the overpotential for the I2M mechanism is much smaller than for the WNA-2 (0.34 versus 1.02 V), suggests that these two mechanisms are at least competitive at a certain temperature.

For the Ir-hyb catalyst, the Pourbaix diagram analysis suggests existence of two different resting states in the range of typical OER overpotentials (purple and gray regions in Figure 2c). Therefore, we have examined the activity of these two species considering both the WNA and I2M mechanisms for each of them. For the two species, we find the same lowest energy paths and potential limiting steps as for the Ir-hom system (Figure S7). In particular, for the Ir-hyb species containing 7H atoms, we find that all the electrochemical steps in the WNA-2 and I2M mechanisms are downhill in energy at the potentials of 2.24 and 1.50 V, respectively (Figure S8). However, the I2M mechanism is further hampered by the high chemical energy required to form the μ-1,2-peroxo intermediate (0.98 eV).

On the other hand, for the Ir-hyb species with 6H atoms, all the electrochemical steps in the WNA-2 and I2M mechanisms become downhill at 2.18 and 1.76 V, respectively. In this case, we find that the formation energy for the μ-1,2-peroxo intermediate is rather small (0.39 eV), and therefore, it may be surpassed even at room temperature. Based on this thermodynamic data, we predict that the I2M mechanism for this species may be more favorable than WNA-2. In other words, the height of the chemical step and the overpotential for the WNA-2 mechanism for this species are lower than for the one containing 7H atoms, which suggests that Ir-hyb with 6H atoms may be more representative for the OER activity of this catalyst.

Taken together, our results show that the intrinsic OER activity of the different model Ir-based catalysts via a WNA-2 mechanism increases as follows: Ir-hom ≈ Ir-hyb < Ir-het. With regards to the I2M mechanism, the comparison between the Ir-hom and Ir-hyb systems is more complicated due to the concurrence of electrochemical and chemical reaction steps. Nevertheless, the fact that Ir-hom requires a slightly lower overpotential compared to Ir-hyb (0.34 V versus 0.53 V), but a higher energy chemical step (0.59 eV versus 0.39 eV), indicates that these two catalysts might exhibit a comparable OER activity. The comparison of the overall activity between the three model Ir-based catalysts is also rather complex, as the lowest energy-demanding pathway for both Ir-hom and Ir-hyb is the I2M which involves a chemical step, whereas for Ir-het it is the WNA-2 mechanism. If we assume the same surmountable barrier for the chemical steps for Ir-hom and Ir-hyb, the activity trend is then dictated by the applied overpotential: Ir-het ≈ Ir-hom ≥ Ir-hyb. Although this trend is not conclusive, the high OER activity predicted for Ir-hom would support that this species might be part of the purple-blue solution, as suggested by Crabtree *et al*.[47] However, we note that the same authors also proposed that this species eventually form IrO_2 nanoparticles, and thus it might not be very stable in aqueous solution in agreement with the exothermic value we have obtained for the adsorption of the dimer on the IrO_2 surface in Eq. (1).

Finally, in order to shed light on the role of the surface in Ir-hyb, we have performed the Bader charge analysis that is presented in Figure 4. We find that the electronic charge of the O atoms in the resting states of the different Ir-based catalysts (top axial oxo-groups) increase in the order: $|q_{Ir\text{-}het}| < |q_{Ir\text{-}hyb}| \approx |q_{Ir\text{-}hom}|$. This indicates that the oxo-moieties in the Ir-hyb and Ir-hom catalysts are less electrophilic than in Ir-het. Consequently, oxo-groups in Ir-hom and Ir-hyb are less reactive towards the nucleophilic attack of a water molecule, which accounts for the predicted activity trend via the WNA-2 mechanism. In addition,

we find that the charge of the Ir atoms of the active site varies within the different model catalysts, pointing to an increase in oxidation state as follows: Ir-het < Ir-hyb < Ir-hom. This trend is tightly coupled to the electronic charge of the O atoms involved in the reaction. We also observe that the charge of the O-linkers of Ir-hyb and the bottom oxo-moieties in Ir-hom (Figures 4a,b) are similar, thus suggesting that the former behave more similarly to oxo-ligands rather than hydroxo groups (Figure S9). This can be ascribed to the additional charge donation provided

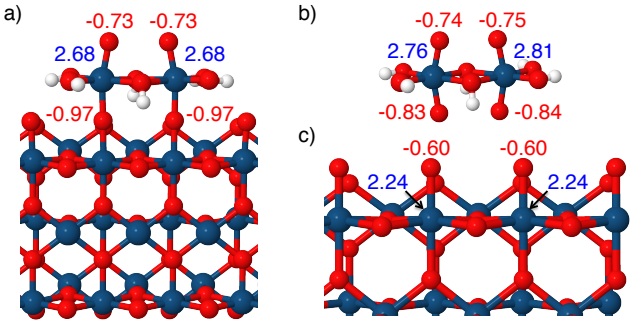

by the IrO_2(110) surface to the O-linkers in the Ir-hyb catalyst.

Figure 4. Calculated oxygen (red) and iridium (blue) Bader charges in $|e^-|$ for the resting states of the (a) Ir-hyb, (b) Ir-hom, and (c) Ir-het catalysts.

Conclusions

In this work, we have employed Density Functional Theory calculations to evaluate the viability of a hybrid water oxidation catalyst generated by attaching a dimeric Ir complex to the IrO_2(110) surface. Our results indicate that the interaction between the adsorbed catalyst and the surface is rather strong as a result of the electron donation from both Ir atoms in the anchored complex and the surface, to the O linkers. The OER activity of the Ir-hyb catalyst is further assessed and compared to its constituent fragments. The activity trend for the WNA mechanism is Ir-hom ≈ Ir-hyb < Ir-het. Assuming that the Ir-hyb system has a similar chemical barrier for the I2M mechanism than the one calculated for Ir-hom, the overall catalytic activity may be governed by the applied potential, thus resulting in the following trend: Ir-het ≈ Ir-hom ≥ Ir-hyb. The high activity of Ir-hom shown in our calculations is consistent with the similar structures suggested to be involved in the formation of the purple-blue solution.[47] Importantly, our calculations predict no significant activity loss when the dimeric Ir complex is anchored on the IrO_2(110) surface through O atoms. Thus, by attaching the dimeric Ir complex to an IrO_2(110) surface through O-linkers, the stability of the homogeneous catalyst might be enhanced, as calculations show that this interaction is very strong.

Taken together, the results reported herein are encouraging as they suggest that hybrid catalysts are not only viable, but they might also benefit from the activity of homogeneous catalysts and the stability of heterogeneous ones. Our findings are in line with very recent experimental findings of stable and water oxidation active dimeric Ir complex anchored on a metal oxide surface.[34] The here demonstrated phenomena for an Ir oxide based hybrid system should be generalizable to more affordable materials. Furthermore, our findings suggest that there is ample of room to improve the catalytic performance of hybrid catalysts by fine-tuning the ligands of the homogeneous constituent and the electro-chemical properties of the heterogeneous constituent.

Acknowledgements

The authors acknowledge support from the DOE Office of Basic Energy Science to the SUNCAT Center for Interface Science and Catalysis and SLAC National Accelerator Laboratory LDRD program. M.G.-M. acknowledges funding from the Agency for Administration of University and Research Grants of Catalonia (AGAUR, 2013 BP-A 00464). L.V. acknowledges funding from MINECO (CTQ2014-54071-P) and MECD (FPU fellowship). N.L. acknowledges funding from MINECO (CTQ2012-33826/BQU). The authors would like to thank Prof. Jens K. Nørskov and Dr. Michal Bajdich for helpful discussions.

Keywords: Oxygen evolution reaction • water oxidation • density functional theory • Ir-catalyst • homogeneous • heterogeneous • hybrid systems • reaction mechanisms

[1] T. B. Johansson, *Renewable energy: sources for fuel and electricity*; Island press: Washington, D.C., 1993.
[2] *Energy Environ. Sci.* **2010**, *3* (2), 173–173.
[3] D. Gust, T. A. Moore, A. L. Moore, *Acc. Chem. Res.* **2009**, *42* (12), 1890–1898.
[4] K. S. Joya, Y. F. Joya, K. Ocakoglu, R. van de Krol, *Angew. Chem. Int. Ed.* **2013**, *52* (40), 10426–10437.
[5] I. Katsounaros, S. Cherevko, A. R. Zeradjanin, K. J. J. Mayrhofer, *Angew. Chem. Int. Ed.* **2014**, *53* (1), 102–121.
[6] H. Dau, C. Limberg, T. Reier, M. Risch, S. Roggan, P. Strasser, *ChemCatChem* **2010**, *2* (7), 724–761.
[7] H. Inoue, T. Shimada, Y. Kou, Y. Nabetani, D. Masui, S. Takagi, H. Tachibana, *ChemSusChem* **2011**, *4* (2), 173–179.
[8] L. Duan, F. Bozoglian, S. Mandal, B. Stewart, T. Privalov, A. Llobet, L. Sun, *Nat. Chem.* **2012**, *4* (5), 418–423.
[9] C. C. L. McCrory, S. Jung, I. M. Ferrer, S. M. Chatman, J. C. Peters, T. F. Jaramillo, *J. Am. Chem. Soc.* **2015**, *137* (13), 4347–4357.
[10] J. D. Blakemore, R. H. Crabtree, G. W. Brudvig, *Chem. Rev.* **2015**, *115* (23), 12974–13005.
[11] A. Llobet, *Molecular Water Oxidation Catalysis*; John Wiley & Sons, Ltd, 2014.
[12] P. C. K. Vesborg, T. F. Jaramillo, *RSC Adv.* **2012**, *2* (21), 7933–7947.
[13] R. Tagore, R. H. Crabtree, G. W. Brudvig, *Inorg. Chem.* **2008**, *47* (6), 1815–1823.
[14] C. S. Mullins, V. L. Pecoraro, *Coord. Chem. Rev.* **2008**, *252* (3-4), 416–443.
[15] C. Zhang, C. Chen, H. Dong, J.-R. Shen, H. Dau, J. Zhao, *Science* **2015**, *348* (6235), 690–693.
[16] M. W. Kanan, D. G. Nocera, *Science* **2008**, *321* (5892), 1072–1075.
[17] P. Du, R. Eisenberg, *Energy Environ. Sci.* **2012**, *5* (3), 6012–6021.
[18] J. A. Haber, Y. Cai, S. Jung, C. Xiang, S. Mitrovic, J. Jin, A. T. Bell, J. M. Gregoire, *Energy Environ. Sci.* **2014**, *7* (2), 682–688.
[19] D. Friebel, M. W. Louie, M. Bajdich, K. E. Sanwald, Y. Cai, A. M. Wise, M.-J. Cheng, D. Sokaras, T.-C. Weng, R. Alonso-Mori, R. C. Davis, J. R. Bargar, J. K. Nørskov, A. Nilsson, A. T. Bell, *J. Am. Chem. Soc.* **2015**, *137* (3), 1305–1313.

[20] M. García-Mota, A. Vojvodic, F. Abild-Pedersen, J. K. Nørskov, *J. Phys. Chem. C* **2013**, *117* (1), 460–465.

[21] G. Novell-Leruth, G. Carchini, N. López, *J. Chem. Phys.* **2013**, *138* (19), 194706.

[22] E. W. McFarland, H. Metiu, *Chem. Rev.* **2013**, *113* (6), 4391–4427.

[23] K. Fominykh, P. Chernev, I. Zaharieva, J. Sicklinger, G. Stefanic, M. Döblinger, A. Müller, A. Pokharel, S. Böcklein, C. Scheu, T. Bein, D. Fattakhova-Rohlfing, *ACS Nano* **2015**, *9* (5), 5180–5188.

[24] J. Suntivich, E. E. Perry, H. A. Gasteiger, Y. Shao-Horn, *Electrocatalysis* **2012**, *4* (1), 49–55.

[25] M. Wiechen, I. Zaharieva, H. Dau, P. Kurz, *Chem. Sci.* **2012**, *3* (7), 2330–2339.

[26] B. Li, F. Li, S. Bai, Z. Wang, L. Sun, Q. Yang, C. Li, *Energy Environ. Sci.* **2012**, *5* (8), 8229–8233.

[27] A. D. Doyle, J. H. Montoya, A. Vojvodic, *ChemCatChem* **2015**, *7* (5), 709–709.

[28] J. J. Concepcion, R. A. Binstead, L. Alibabaei, T. J. Meyer, *Inorg. Chem.* **2013**, *52* (19), 10744–10746.

[29] D. K. Zhong, S. Zhao, D. E. Polyansky, E. Fujita, *J. Catal.* **2013**, *307*, 140–147.

[30] B. M. Klepser, B. M. Bartlett, *J. Am. Chem. Soc.* **2014**, *136* (5), 1694–1697.

[31] G. Li, E. M. Sproviero, R. C. Snoeberger III, N. Iguchi, J. D. Blakemore, R. H. Crabtree, G. W. Brudvig, V. S. Batista, *Energy Environ. Sci.* **2009**, *2*, 230–238.

[32] E. Farnetti, R. Di Monte, J. Kašpar, In *Inorganic and Bio-inorganic Chemistry*; Eolss Publishers: Oxford, UK, 2007; Vol. II.

[33] A. Savini, A. Bucci, M. Nocchetti, R. Vivani, H. Idriss, A. Macchioni, *ACS Catal.* **2015**, *5* (1), 264–271.

[34] S. W. Sheehan, J. M. Thomsen, U. Hintermair, R. H. Crabtree, G. W. Brudvig, C. A. Schmuttenmaer, *Nat. Commun.* **2015**, *6*. 6469.

[35] J. K. Nørskov, J. Rossmeisl, A. Logadottir, L. Lindqvist, J. R. Kitchin, T. Bligaard, H. Jónsson, *J. Phys. Chem. B* **2004**, *108* (46), 17886–17892.

[36] Perdew, J. P.; Burke, K.; Ernzerhof, M. *Phys. Rev. Lett.* **1996**, *77* (18), 3865–3868.

[37] G. Kresse, J. Furthmüller, *Phys. Rev. B* **1996**, *54* (16), 11169–11186.

[38] G. Kresse, J. Furthmüller, *Comput. Mater. Sci.* **1996**, *6* (1), 15–50.

[39] P. E. Blöchl, *Phys. Rev. B* **1994**, *50* (24), 17953–17979.

[40] H. Zhang, A. Soon, B. Delley, C. Stampfl, *Phys. Rev. B* **2008**, *78* (4), 045436.

[41] F. G. Sen, A. Kinaci, B. Narayanan, S. K. Gray, M. J. Davis, S. K. R. S. Sankaranarayanan, M. K. Y. Chan, *J. Mater. Chem. A* **2015**, *3*, 18970–18982.

[42] A. A. Bolzan, C. Fong, B. J. Kennedy, C. J. Howard, *Acta Crystallogr. Sect. B* **1997**, *53* (3), 373–380.

[43] Y. Lee, J. Suntivich, K. J. May, E. E. Perry, Y. Shao-Horn, *J. Phys. Chem. Lett.* **2012**, *3* (3), 399–404.

[44] J. Rossmeisl, A. Logadottir, J. K. Nørskov, *Chem. Phys.* **2005**, *319* (1-3), 178–184.

[45] S. Klüpfel, P. Klüpfel, H. Jónsson, *J. Chem. Phys.* **2012**, *137* (12), 124102.

[46] G. Henkelman; B. P. Uberuaga; H. Jońsson. *J. Chem. Phys.* **2000**, *113* (22), 9901−9904.

[47] U. Hintermair, S. M. Hashmi, M. Elimelech, R. H. Crabtree, *J. Am. Chem. Soc.* **2012**, *134* (23), 9785–9795.

[48] J. D. Blakemore, M. W. Mara, M. N. Kushner-Lenhoff, N. D. Schley, S. J. Konezny, I. Rivalta, C. F. A. Negre, R. C. Snoeberger, O. Kokhan, J. Huang, A. Stickrath, L. A. Tran, M. L. Parr, L. X. Chen, D. M. Tiede, V. S. Batista, R. H. Crabtree, G. W. Brudvig, *Inorg. Chem.* **2013**, *52* (4), 1860–1871.

[49] S. Romain, L. Vigara, A. Llobet, *Acc. Chem. Res.* **2009**, *42* (12), 1944–1953.

[50] X. Sala, S. Maji, R. Bofill, J. García-Antón, L. Escriche, A. Llobet, *Acc. Chem. Res.* **2014**, *47* (2), 504–516.

[51] C. C. L. McCrory, S. Jung, J. C. Peters, T. F. Jaramillo, *J. Am. Chem. Soc.* **2013**, *135* (45), 16977–16987.

[52] J. Rossmeisl, Z.-W. Qu, H. Zhu, G.-J. Kroes, J. K. Nørskov, *J. Electroanal. Chem.* **2007**, *607* (1–2), 83–89.

[53] I. C. Man, H.-Y. Su, F. Calle-Vallejo, H. A. Hansen, J. I. Martínez, N. G. Inoglu, J. Kitchin, T. F. Jaramillo, J. K. Nørskov, J. Rossmeisl, *ChemCatChem* **2011**, *3* (7), 1159–1165.

[54] S. Siahrostami, A. Vojvodic, *J. Phys. Chem. C* **2015**, *119* (2), 1032–1037.

[55] Y. Gong, M. Zhou, M. Kaupp, S. Riedel, *Angew. Chem. Int. Ed.* **2009**, *48* (42), 7879–7883.

[56] G. Wang, M. Zhou, J. T. Goettel, G. J. Schrobilgen, J. Su, J. Li, T. Schlöder, S. Riedel, *Nature* **2014**, *514* (7523), 475–477.

[57] M. García-Mota, A. Vojvodic, H. Metiu, I. C. Man, H.-Y. Su, J. Rossmeisl, J. K. Nørskov, *ChemCatChem* **2011**, *3* (10), 1607–1611.

[58] Y.-H. Fang, Z.-P. Liu, *J. Am. Chem. Soc.* **2010**, *132* (51), 18214–18222.

Entry for the Table of Contents

A Density Functional Theory study has been carried out to compare the stability and activity of a model hybrid water oxidation catalyst with its homogeneous and heterogeneous constituents. Calculations show that homogeneous catalysts can be bound to its matrix oxide without losing significant activity, thus opening the way for the design of hybrid materials that benefit from the properties of both types of catalysts.

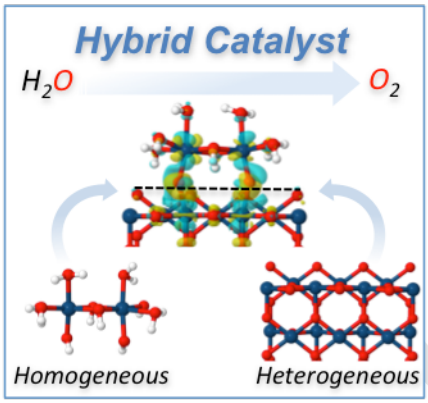

Max García-Melchor, Laia Vilella, Núria López, Aleksandra Vojvodic**

Page 1 – Page 8

Computationally Probing the Performance of Hybrid, Heterogeneous and Homogeneous Ir-based Catalysts for Water Oxidation